Biosensors and Bioelectronics 142 (2019) 111556

Contents lists available at ScienceDirect

Biosensors and Bioelectronics

journal homepage: www.elsevier.com/locate/bios

A label-free immunosensor based on PtPd NCs@MoS_2 nanoenzymes for hepatitis B surface antigen detection

Zhaoling Tan[a], Hui Dong[a], Qing Liu[a,*], Hui Liu[a], Pingping Zhao[b], Ping Wang[a], Yueyun Li[a], Daopeng Zhang[a], Zengdian Zhao[a], Yunhui Dong[a]

[a] School of Chemistry and Chemical Engineering, Shandong University of Technology, Zibo, 255049, PR China
[b] College of Chemical and Environmental Engineering, Shandong University of Science and Technology, PR China

ARTICLE INFO

Keywords:
Nanoenzymes
Peroxidase-like activity
PtPd NCs@MoS_2
Hepatitis B surface antigen

ABSTRACT

Nowadays, nanomaterials with enzymatic properties have aroused wide interest because of their special advantages, such as catalytic activity, simple preparation method and high stability. We introduced new nanoenzymes to a label-free electrochemical immunosensor for Hepatitis B surface antigen (HBs Ag) detection. In this study, PtPd nanocubes@MoS_2 nanoenzymes (PtPd NCs@MoS_2) were prepared by loading PtPd nanocubes (PtPd NCs) on molybdenum disulfide nano-sheet (MoS_2) through in situ redox polymerization. The prepared nanoenzymes exhibited enhanced peroxidase-like activity than separate MoS_2 and PtPd NCs. The catalytic process of PtPd NCs@MoS_2 is in agreement with the Michaelis-Menten kinetic equation. PtPd NCs@MoS_2 were used for sensitive detection of HBs Ag, which is ascribed to their superior peroxidase activity, good conductivity and high specific surface area and synergistic amplification for current signals. Compared with the detection limit of colorimetric method (3.3 pg/mL), the electrochemical method (10.2 fg/mL) shows a lower detection limit and a wider linear range from 32 fg/mL to 100 ng/mL, so it is more suitable for quantitative analysis of Hepatitis B. In summary, the prepared immunosensor provides a better opportunity for early diagnosis of Hepatitis B and also has further applications in biosensing and medical diagnostics.

1. Introduction

Hepatitis B virus (HBV) is one of the most serious diseases worldwide leading to liver cancer and cirrhosis to a large extent (Cho et al., 2018). Hepatitis B surface antigen (HBs Ag) was the first discovered hepatitis B virus (HBV) protein which can evade the patient's immune response (Yan et al., 2018). Detection of HBs Ag is an effective method for identifying chronic HBV because it is long-lasting and almost impossible to lose in chronic cases (Ott et al., 2012). Therefore, rapid and accurate quantitative detection of HBs Ag is important for early diagnosis of HBV infection. Currently, there are various methods for detecting HBs Ag such as enzyme linked immunosorbent assays (ELISA) (Makuza et al., 2019), chemiluminescent microparticle immunoassay (Alzahrani et al., 2019), radioimmunoassay (Hu et al., 2019), reflectometry interference spectroscopy (Yu et al., 2000), gap ligase chain reaction assay (Carla, 2002) and electrochemical immunosensor (Pei et al., 2019). Among these methods, electrochemical immunosensors are considered to be a promising diagnostic method and mainly with the following two reasons: firstly, the electrochemical instrument has the characteristics of miniaturization and easy operation; secondly, the electroanalytical method is simple, convenient, specific and environmental friendly (Yan et al., 2019b; Yang et al., 2018). Especially, the label-free electrochemical immunosensor is widely used due to its simple operation and easy preparation (Wang et al., 2018; Yang et al., 2017).

In recent years, enzymes based on nanomaterials (nanoenzymes) are rapidly developing. Since the disadvantages of the natural enzyme are high cost and poor long-term stability, nanoenzymes with high stability and easy functionalization are prepared. New nanoenzymes such as Pt nanoparticles (Kai et al., 2013), Au nanoparticles (Wang et al., 2011), CuS (He et al., 2012), Co_3O_4 nanoparticles (Jia et al., 2016) and carbon nanomaterials (Li et al., 2013), have been reported to use in biotechnology and environmental control. Nanoenzymes with significant catalytic activity and excellent biocompatibility can be applied in electrochemical immunosensors to improve the sensitivity (Zhang et al., 2019).

The two-dimensional (2D) transition metal disulfide MoS_2 is single sandwiched S–Mo–S layer bound by van der Waals force in a hexahedral filled structure (Gourmelon et al., 2017). Because of the properties such as the indirect band gap, unique layered structure, large specific

* Corresponding author.
E-mail address: qingliu0315@163.com (Q. Liu).

https://doi.org/10.1016/j.bios.2019.111556
Received 6 May 2019; Received in revised form 26 July 2019; Accepted 29 July 2019
Available online 01 August 2019
0956-5663/

surface area, excellent mechanical hardness and good catalytic performance. MoS_2 has shown very good application prospects in many fields such as photocatalysis, super capacitor, biology and batteries (Singh et al., 2018). Besides, inserting other materials into the layered MoS_2 nanosheets to form a hybrid nanomaterial system would enhance conductivity and stimulate new reaction sites (Francesco et al., 2015). Due to the two-dimensional MoS_2 nanosheet with pleated structure, large specific surface area, easy preparation and storage, it was used as platforms for supporting nanoparticles to achieve electrochemical sensing (Duan et al., 2014; Jiang et al., 2019).

In recent years, noble metal nanoparticles have shown excellent electrochemical properties, which are widely used in electrochemical immunosensors. Pt-based nanoparticles exhibit excellent catalytic performance by introducing other elements such as Pd with good catalytic properties (Gao et al., 2014; Shi et al., 2019). The shape of nanomaterials affects their physical and chemical properties (Gomathi et al., 2019). Nanocubic materials have attracted the attention of researchers. Compared with spherical particles, cubic Pt nanoparticles have superior catalytic performance probably because of more active sites (Wang et al., 2008; Yamada, 2009). This is the first time that PtPd NCs have been found to catalyze the oxidation of TMB tetramethylbenzidine (TMB) by H_2O_2 to produce blue TMB oxide (TMB ox), demonstrating its unique peroxidase activity used as nanoenzymes. We designed PtPd nanocubes (PtPd NCs), which obtained unique catalytic activity because of large cubes stacked by small cubes, and then loaded them onto MoS_2 nanosheets as effective nanoenzymes for the preparation of electrochemical immunosensors.

The prepared label-free immunosensor amplifies the signal with PtPd nanocube@MoS_2 nanoenzymes (PtPd NCs@MoS_2) for HBs Ag detection. Since antigens and antibodies cannot undergo redox in the immunoassay reaction, differential pulse voltammetry (DPV) was used to detect the electrical signal generated by PtPd NCs@MoS_2 nanoenzyme catalyzing the oxidation of phenylenediamine (o-PD) by H_2O_2 in this study. PtPd NCs have excellent electrical conductivity and biocompatibility and are easily bound to antibodies by Pt–N bonds (Li et al., 2019) and Pd–N bonds (Yan et al., 2019a), which is more conducive to increase the amount of bound antibody. MoS_2 with a pleated paper structure has a large specific surface area, which allows it to successfully load PtPd NCs to achieve synergistic amplification of electrochemical signals. The PtPd NCs@MoS_2 nanocomposites exhibit enhanced electrical conductivity and catalytic activity. Thus, we applied PtPd NCs@MoS_2 to electrochemical immunosensors to increase substrate reaction rate and electron transfer efficiency, and further improve the sensitivity of the immunosensor (Fig. 1). Besides, MoS_2 has inherent peroxidase activity (Ma et al., 2019), and successfully loading PtPd NCs can achieve enhanced peroxidase performance. Due to the synergistic effect of the composite nanoenzymes, PtPd NCs@MoS_2 can also be applied to in situ colorimetric analysis. The contrast between the two methods convincingly demonstrates the advantages of electrochemical analytical methods.

2. Experimental section

2.1. Reagents

Hexachloplatinic (IV) acid hexahydrate ($H_2PtCl_6{\cdot}6H_2O$, 99.9%), palladium (II) chloride ($PdCl_2$, 99.9%), poly (vinylpyrrolidone) (PVP, Mw ≈ 29000), KI (AR), O-phenylenediamine (o-PD), ethylene glycol (EG, AR), HCl, 3,3′,5,5′-Tetramethylbenzidine (TMB), terephthalic acid (TA), Sodium molybdate dehydrate ($Na_2MoO_4{\cdot}2H_2O$), L-cysteine were obtained from Sinopharm Chemical Reagent Co., Ltd. Bovine serum albumin (BSA), HBs Ag and HBs antibody (anti-HBs) were bought from Shanghai Linc-Bio Science Co., Ltd. Ultrapure water was used in the whole experiment.

2.2. Apparatus

The CHI760E electrochemical workstation was used to measure electrochemical performance. Transmission electron microscope (TEM) images were obtained from JEOL JSM-6700F microscope and energy-dispersive X-ray spectroscopy (EDX) analysis were collected by a Tecnai G2 F20 (America). UV–visible spectroscopy analysis was conducted by Agilent Technologies Cary 60 UV–Vis. Fluorescence analysis was collected by F-380 fluorescence spectrophotometer.

2.3. Preparation of MoS_2

The preparation of MoS_2 was based on the literature with some modifications (Wang et al., 2016). The $Na_2MoO_4{\cdot}2H_2O$ (0.25 g) was dissolved in water and maintained at pH 6.5. L-cysteine (0.5 g) and water (50 mL) were added to the solution sonicating for 10 min. The precursor solution was transferred into a 100 mL Teflon-lined stainless steel autoclave. The autoclave was sealed and maintained at 200 °C for 18 h and then cooled to room temperature. The MoS_2 were collected through centrifugation at the speed of 7000 rpm.

2.4. Preparation of the PtPd NCs and PtPd NCs@MoS_2

The preparation method of PtPd NCs has been referred to the literature and modified (Zhou et al.) and the method for PtPd NCs@MoS_2 is as followed: The H_2PdCl_4 solution (20 mM, 0.5 mL) and H_2PtCl_6 solution (20 mM, 0.5 mL) were added into 20 mL EG containing PVP (160 mg). The KI aqueous solution (5 M, 110 μL) and the obtained MoS_2 nanosheets were added into mixed solution. Subsequently, the mixture was heated to 150 °C with vigorous stirring. The product was collected by centrifugation at 5000 rpm and washed with ethanol and water and then dispersed in ethanol.

2.5. Peroxidase activity and color reaction

The enhanced peroxidase activity of the composed nanoenzymes we produced was confirmed by color reaction. The reaction substrate 5 mmol/L of TMB was catalytically oxidized by adding 5.0 mmol/L of H_2O_2 and 5 μg/mL of MoS_2, PtPd NCs, PtPd NCs@MoS_2, respectively, resulting in a blue reaction. To obtain the Michaelis-Menten equation, the gradient concentrations of H_2O_2 were set to measure its reaction rate. We calculated the Michaelis constants V_m and K_m by plotting the double reciprocal curves where V_m represents the maximum rate of enzymatic reaction, and the smaller the K_m, the greater the affinity of the enzyme (Liu et al., 2016).

$$\text{Michaelis} - \text{Menten equation:} \frac{1}{v} = \frac{K_m}{V_m}\left(\frac{1}{[S]} | \frac{1}{K_m}\right)$$

2.6. Fabrication of the PtPd NCs@MoS_2 immunosensor

Fig. 1 illustrates the preparation process of immunosensor based on PtPd NCs@MoS_2 nanoenzymes. The specific preparation method is as follows: the surface of the glassy carbon electrode (GCE) is polished by Al_2O_3 powder with diameters of 1.0, 0.3 and 0.05 mm, respectively and then washed. 2.2 mg/mL of PtPd NCs@MoS_2 (6 μL) nanoenzyme was coated onto the treated GCE and dried in air. The prepared PtPd NCs@MoS_2/GCE was incubated with 10 μg/mL of anti-HBs (6 μL), followed by drying treatment at 4 °C. The unsuccessfully bound antibody was washed away with phosphate buffer solution (PBS) and dried at 4 °C. BSA solution (3 μL, 1 wt%) can block non-specific sites and exclude other non-specific binding interference. After drying, the prepared anti-HBs/BSA/PtPd NCs@MoS_2/GCE was incubated with a gradient concentration of 6 μL of HBs Ag (32 fg/mL - 100 ng/mL) to complete the specific immunological binding and dried at 4 °C. Finally, the

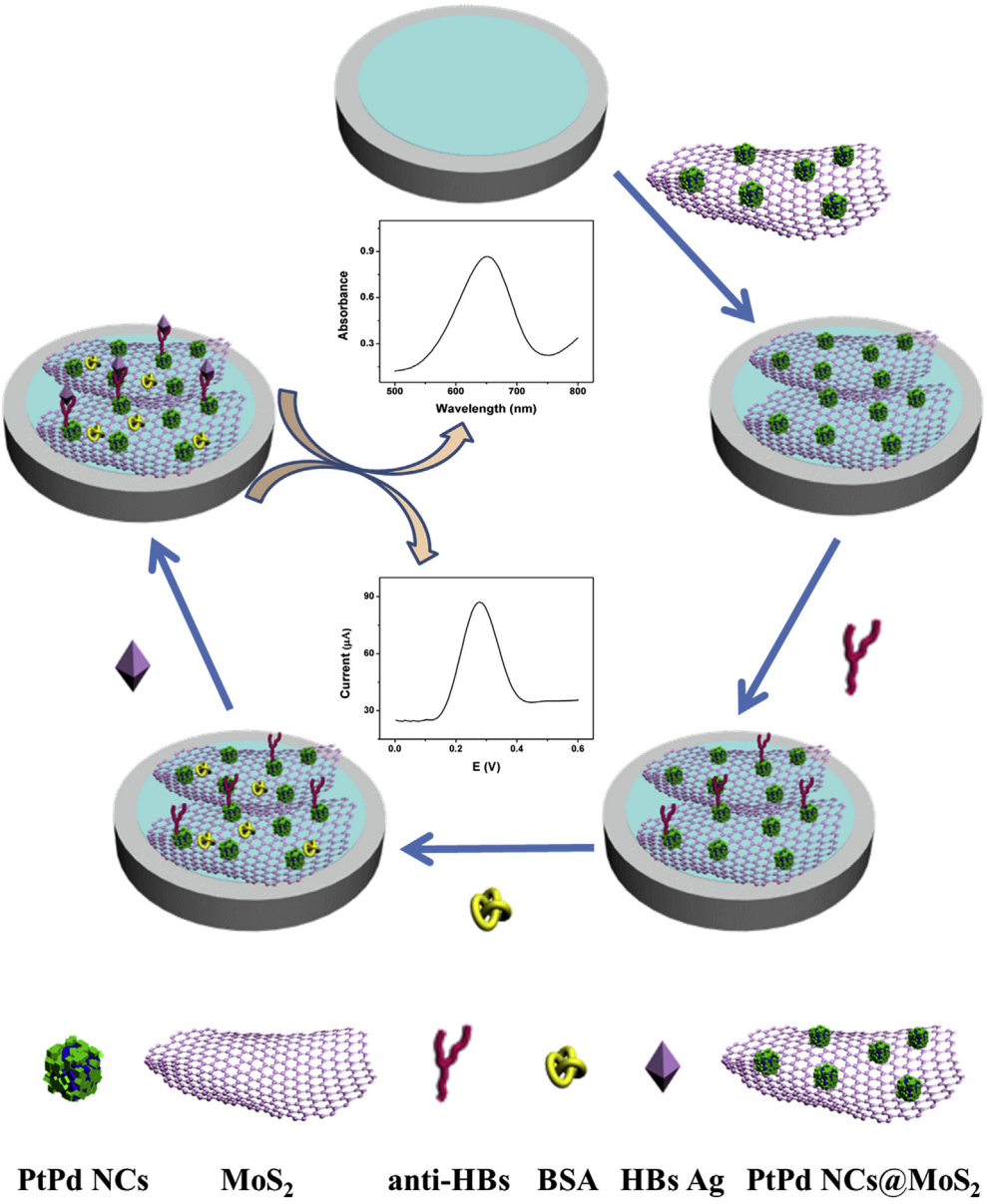

Fig. 1. Schematic illustration of PtPd NCs@MoS_2 for the detection of HBs Ag and signal response mechanism.

unsuccessfully bound antigen was washed away and the prepared immunosensor was stored for subsequent use at 4 °C.

2.7. Electrochemical measurements

A saturated calomel electrode and a platinum wire electrode were used as a reference electrode and a counter electrode, respectively. Amperometric i-t measurement were conducted by adding H_2O_2 (5 mmol/L) into PBS (10 mL, pH = 7.0) at 60 s, 120 s and 180 s, respectively. CV was tested at the rate of 0.1 V/s and EIS is with the frequency from 0.1 Hz to 100 kHz at a bias potential of 0.23 V in 0.1 mol/L KCl containing 2.5 mmol/L $[Fe(CN)_6]^{3-/4-}$. All DPV measurements were performed with the voltage ranging from 50 mV to 650 mV, with a pulse amplitude of 50 mV, pulse width of 50 m s, pulse period of 500 m s with 10 mL PBS (pH = 7.0), o-PD (2.0 mmol/L) and H_2O_2 (5.0 mmol/L) in system.

2.8. Colorimetric detection

After DPV measurement, the prepared series of immunosensors washing with PBS were placed in 600 μL of 5 mmol/L TMB, 200 μL of 10 mmol/L H_2O_2 and 300 μL of PBS (pH = 7) and fixed, and incubated for 3 min at room temperature in the dark. In order to stop the reaction, we only need to remove the immunosensor from the solution. To demonstrate the relationship between absorbance and antigen concentration, absorbance curves at the wavelength of 652 nm were determined using Agilent Technologies Cary 60 UV–Vis (Beckman Coulter, USA).

3. Results and discussion

3.1. Characterization of PtPd NCs@MoS_2

As shown in Fig. 2A, MoS_2 nanosheets have a pleated paper-like structure which looks like an ink painting. Fig. 2B shows PtPd NCs with an average side length of about 50 nm. We can see that the surface of PtPd NCs is not flat because it is composed of smaller nanocubes instead of cubic nanosheets. There is only square structure without a linear structure by observation, so it cannot be formed by stacking a square sheet structure but by cubic stacking (Fig. S1). Moreover, the cubic

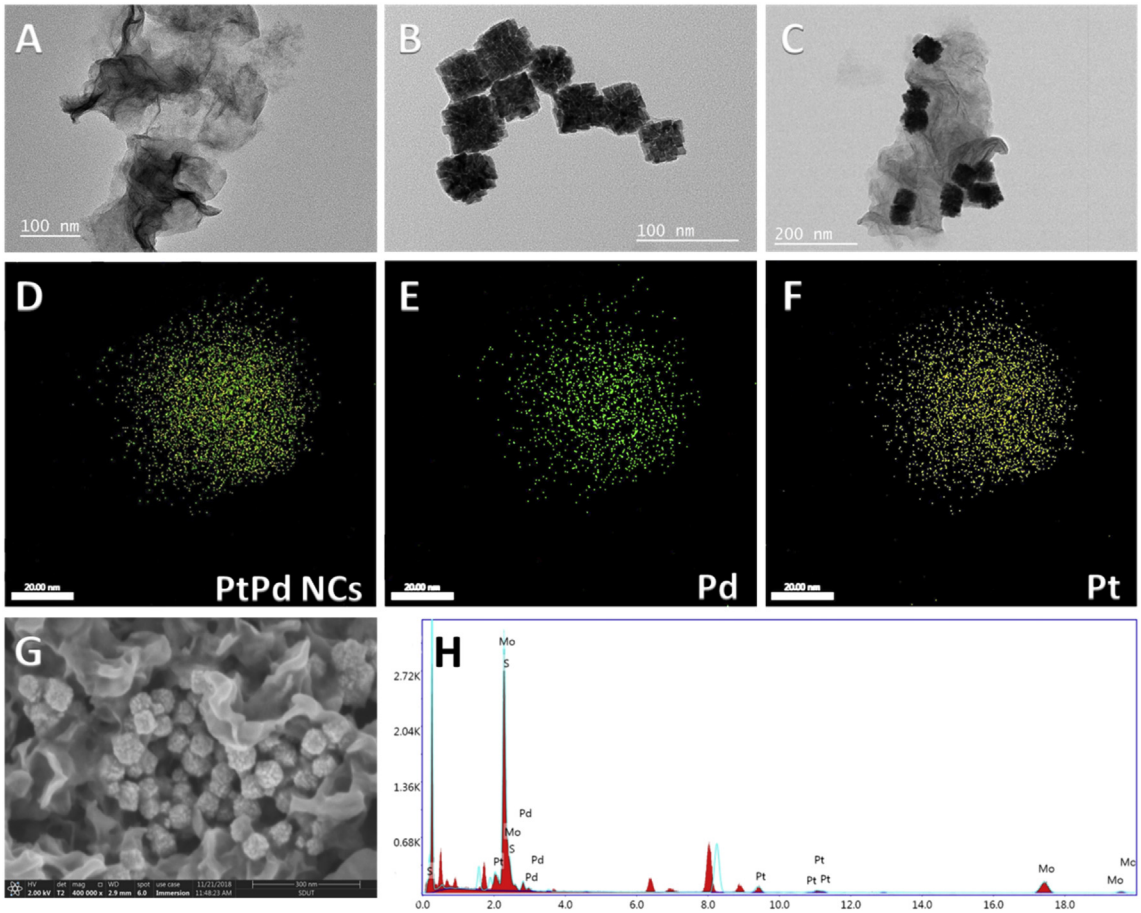

Fig. 2. The TEM images: (A) MoS_2 nanosheets, (B) PtPd NCs, (C) PtPd NCs@MoS_2; The elemental mappings: (D) PtPd NCs, (E) Pd, (F) Pt; The SEM image of PtPd NCs@MoS_2 (G); The EDX spectrum of PtPd NCs@MoS_2 (H).

structure can be basically seen from Fig. 2G. The mapping spectrum of PtPd element (Fig. 2D), Pd (Fig. 2E, yellow) and Pt (Fig. 2F, green) clearly illustrate that the two elements are evenly distributed meaning good alloying of Pt and Pd (Fig. 2D). Two lattice fringes were found: one is ~0.23 nm corresponding to (111) (Fig. S2A), and the other is ~0.19 nm (Fig. S2B), corresponding to (200), which are in good agreement with face-centered cubic Pt and Pd (200) lattice spacing. The low crystallinity at the junction leads to a phenomenon in which the lattice fringes are not obvious at the junction of the small cubes (Fig. S2A). Fig. 2C shows that the prepared PtPd NCs supported on paper-like nanosheets and their EDX spectrum (Fig. 2H), indicating that the composite nanoenzyme contains elements of Mo, S, Pt and Pd. The elements of Mo and S cover the entire composite nanoenzymes and play an important role in supporting the nanocubes (Figs. S3E and S3F). The elemental maps of Mo, S, Pt, Pd and PtPd NCs@MoS_2 indicate the successful preparation of the composite nanoenzymes (Fig. S3B).

3.2. Peroxidase-like properties of PtPd NCs@MoS_2 and catalytic mechanism

The enhanced peroxidase performance of the prepared composite nanoenzymes were demonstrated with TMB as reaction substrates. Because of the special stacked nanocubic structure of PtPd NCs and the synergy with pleated MoS_2, the prepared PtPd NCs@MoS_2 nanoenzymes were first discovered to have enhanced peroxidase performance. As seen from Fig. 3A, the maximum absorption peak of the oxidation product of TMB is at 652 nm in the UV–vis absorption spectra. The reaction color of PtPd NCs@MoS_2 is significantly darker than that of MoS_2 and PtPd NCs, and the absorption peak is the largest, which is related to the amount of blue oxide (TMB ox) indicating the better catalytic performance. In the control experiment, only TMB and H_2O_2 were added without any nanoenzymes, which caused no absorption peaks and color changes, indicating that H_2O_2 spontaneously catalyzed oxidation of TMB was almost negligible, while nanoenzymes could indeed simulate peroxidase-catalyzed oxidation of TMB by H_2O_2. Moreover, steady state kinetics and catalytic activity were further investigated to compare the peroxidase properties of different nanoenzymes by varying the concentration of H_2O_2. The kinetic constants K_m, V_m, and catalytic efficiency k_{cat}/K_m of different nanoenzymes were calculated according to the Michaelis-Menten equation and the double reciprocal curve (Fig. 3B–C). The larger K_m value of PtPd NCs@MoS_2 indicates stronger affinity for H_2O_2 and the larger V_m indicates faster reaction rate (Table S1). Besides, the catalytic efficiency k_{cat}/K_m of PtPd NCs@MoS_2 nanoenzymes is 21.1, which is significantly larger than MoS_2 and PtPd NCs, suggesting that the composite nanoenzymes have higher catalytic activity. Comparison of the above kinetic parameters further indicates that PtPd NCs@MoS_2 has much better peroxidase performance than single PtPd NCs and MoS_2. The prepared PtPd NCs@MoS_2 nanoenzymes with enhanced peroxidase properties may be attributed to unique nanocubic stacking structure and large specific surface area of nanosheets. In brief, PtPd NCs@MoS_2 is an excellent nanoenzyme with high peroxidase efficiency.

To reveal the reaction mechanism of the nanoenzyme, TA was used to capture hydroxyl radicals (·OH) and produced unique fluorescence near 425 nm. As shown in Fig. 3D, the fluorescence intensity of PtPd NCs@MoS_2 system was significantly greater than that of MoS_2 and PtPd NCs. The results not only demonstrate the hydroxyl radical mechanism of the synthesized PtPd NCs@MoS_2 catalytic reaction, but also show

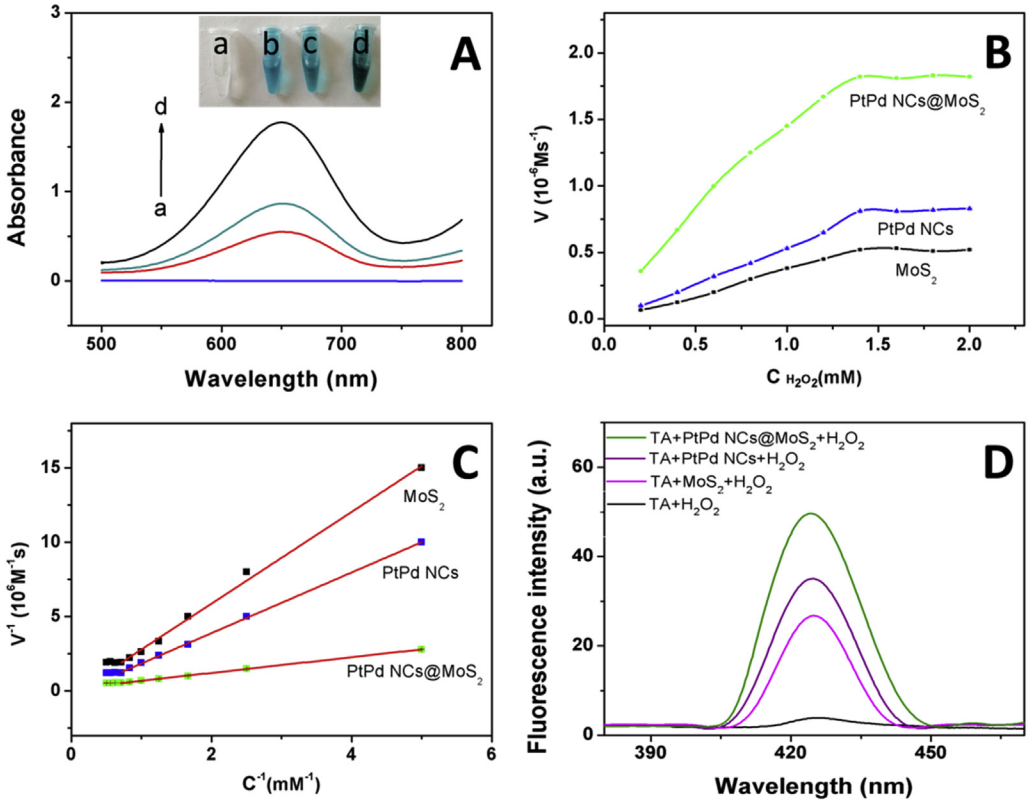

Fig. 3. (A) Photographs and UV–visible absorption curves for oxidation of TMB of different systems (a. H_2O_2 + TMB, b. MoS_2 + H_2O_2 + TMB, c. PtPd NCs + H_2O_2 + TMB d. PtPd NCs@MoS_2 + H_2O_2 + TMB) in PBS (pH = 7.0); (B) Comparison of steady-state kinetics of MoS_2, PtPd NCs and PtPd NCs@MoS_2 in different concentrations of H_2O_2 with 5 mmol/L of TMB; (C) Double reciprocal plots of activity of different nanoenzymes; (D) Fluorescence spectra of interactions between different nanoenzymes and TA with H_2O_2 in system, nanoenzymes (5 μg/mL) incubated with 1.2 mmol/L TA and 0.3 M H_2O_2 in 3 mL of PBS (pH = 7.0).

that the prepared composite nanomaterials have enhanced peroxidase properties, which is consistent with the result of UV–vis spectra analysis.

3.3. Electrochemical characterization

The chronoamperometry method was used to demonstrate the catalytic performance of the designed PtPd NCs@MoS_2 nanoenzymes. As shown in Fig. 4A, PtPd NCs@MoS_2 exhibit much larger current signal than MoS_2 (curve a) and PtPd NCs (curve b) because the unique cubic packing structure of PtPd NCs and the large specific surface area of MoS_2 can increase the reaction site. It further proves that our composite nanoenzymes were successfully prepared and have enhanced catalytic performance. The peak current was almost unchanged after multiple scans, indicating that the prepared PtPd NCs@MoS_2 has good stability (Fig. 4B).

Cyclic voltammetry (CV) and electrochemical impedance spectroscopy (EIS) were used to examine the step-by-step assembly process, further demonstrating the successful construction of the label-free immunosensor (Fig. 4C and D). The EIS consists of a semicircular and linear portion in which the diameter of the semicircle is positively correlated with the electron transfer resistance (R_{et}). The CV of GCE (curve b) has a symmetrical redox peak. After PtPd NCs@MoS_2 modification (curve a), the redox peak current increased significantly and the AC impedance radius decreased significantly due to its good electrical conductivity. With anti-HBs (curve c), BSA (curve d), and HBs Ag (curve e) sequentially loaded, the peak current decreases, and the AC impedance radius increases, which is attributed to the fact that the protein inhibits electron transfer. In summary, a label-free electrochemical immunosensor was successfully manufactured.

In order to study the catalytic process of the prepared composite nanoenzymes, the scanning speed was changed from 0.01 to 0.15 V/s, and the peak current of CV was linear with the square root of the scanning rate, indicating that the reaction process catalyzed by nanoenzymes on the electrode surface was diffusion control (Fig. 4H). We further studied the synergistic amplification effect of the prepared composite nanoenzymes, and analyzed the active area after different nanoenzyme modified electrodes using the Randles-Sevcik equation. Randles-Sevcik equation is shown as follows: $i_p = 2.686 \times 10^5 D^{\frac{1}{2}} n^{\frac{3}{2}} A C v^{\frac{1}{2}}$, the i_p in the formula is the peak current, D is the diffusion coefficient, n is the number of electron transfer, C is the concentration of $K_3[Fe(CN)_6]$, v is the sweep speed, and A is the active area. The effective area ratio of PtPd NCs@MoS_2 and PtPd NCs is $A_{PtPd\ NCs@MoS_2}/A_{PtPd\ NCs} = 1.15$, which means the synergistic effects and larger active area of PtPd NCs@MoS_2 nanoenzyme. Therefore, we chose PtPd NCs@MoS_2 as a signal amplification platform for label-free immunosensors.

3.4. Optimization of experimental condition

In order to get better electrocatalytic signals, we optimized the experimental conditions: pH, the concentration of PtPd NCs@MoS_2 and the amount of anti-HBs. The pH of the PBS is very important for the activity of the immunosensor, as strong acidic or basic conditions may inactivate the antigen and antibody, thereby invalidating specific binding. As the pH increases, the current signal appears to increase first and then decrease. The best current signal is obtained at pH 7.43 because the antigen and antibody maintain good biological activity at this time. Therefore, PBS of pH 7.43 was chosen as the best electrolyte for electrochemical measurements (Fig. S4A).

The concentration of PtPd NCs@MoS_2 can affect the electron transfer rate and the amount of bound antibodies, and as the concentration of PtPd NCs@MoS_2 increases, the site of bound antibodies also increases. To amplify the current signal, more antibodies need to be loaded, so we optimized the concentration of PtPd NCs@MoS_2 and the amount of anti-HBs. The current signal increases first and then remains constant as the concentration of PtPd NCs@MoS_2 increases (Fig. S4B), and the maximum current response is obtained at a concentration of 2.2 mg/mL. When the concentration of PtPd NCs@MoS_2 is 2.2 mg/mL, the maximum current signal can be obtained by changing the

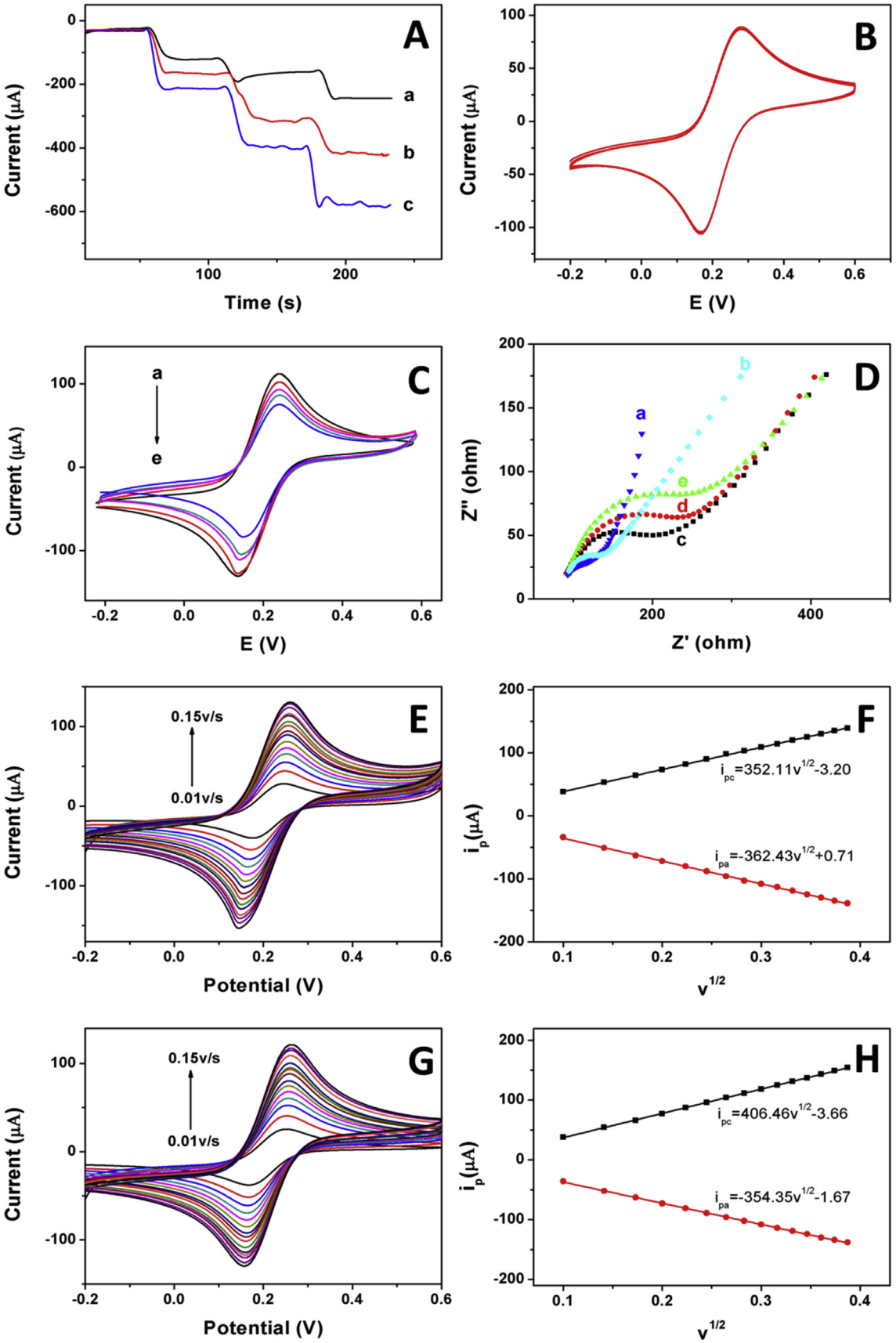

Fig. 4. (A) Ameperometic response: (a) MoS_2, (b) PtPd NCs, (c) PtPd NCs@MoS_2 in 10 mL PBS (pH = 7.38); (B) CV curves of PtPd NCs@MoS_2 at 20 cycles of 0.1 V/s with continuous scanning; (C) CV and (D) EIS of (a) PtPd NCs@MoS_2/GCE, (b) bare GCE, (c) anti-HBs/PtPd NCs@MoS_2/GCE, (d) BSA/anti-HBs/PtPd NCs@MoS_2/GCE, (e) HBs Ag/BSA/anti-HBs/PtPd NCs@MoS_2/GCE; CV curves of electrode modified by (E) PtPd NCs and (G) PtPd NCs@MoS_2 from 0.01 to 0.15 V/s in 0.1 mol/L KCl containing 5.0 mmol/L $K_3[Fe(CN)_6]^{3-/4-}$; The relationship between i_p and $v^{1/2}$ of (F) PtPd NCs and (H) PtPd NCs@MoS_2.

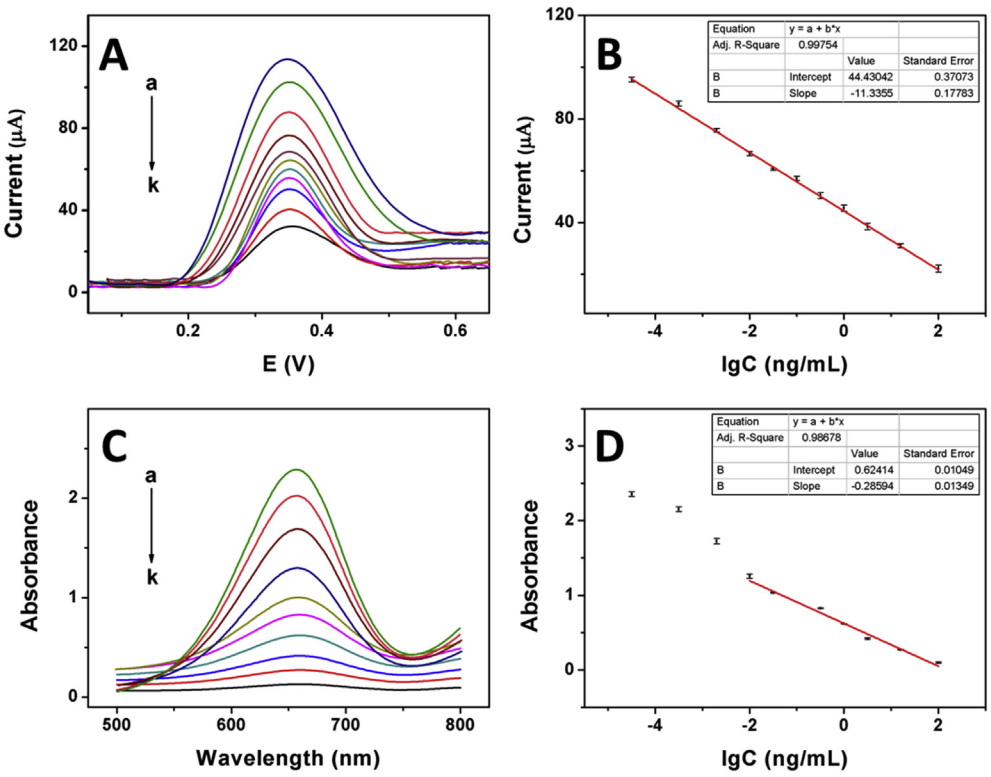

Fig. 5. (A) DPV responses and (C) UV–vis absorption spectra of different concentrations of HBs Ag: (a) 32 fg/mL, (b) 0.32 pg/mL, (c) 2 pg/mL, (d) 10 pg/mL, (e) 31.7 pg/mL, (f) 100 pg/mL, (g) 0.32 ng/mL, (h) 1 ng/mL, (i) 3.2 ng/mL, (j) 15.8 ng/mL, (k) 100 ng/mL; (B) Calibration curve of electrochemical immunosensors, Error bars = RSD (n = 5); (D) Calibration curve of colorimetric method, Error bars = RSD (n = 5).

amount of the anti-HBs added. As can be seen from Fig. S4C, as the amount of anti-HBs added increases, the current signal gradually decreases. When the amount of bound anti-HBs reaches saturation, the current signal remains unchanged. Therefore, the optimal amount of anti-HBs is 6 μL (10 μg/mL). Detailed experiments were displayed in supporting information.

3.5. Analytical performance of immunosensor

We have used PtPd NCs@MoS_2 nanoenzymes with excellent catalytic activity and conductivity to fabricate electrochemical immunosensors. DPV was chosen as the electrochemical detection method instead of other method because it can effectively reduce the background current due to the subtraction of the capacitive current. In order to demonstrate the excellent detection limits and sensitivity of the prepared electrochemical immunosensors, PtPd NCs@MoS_2 nanoenzymes were used in colorimetric sensors for comparison. As the antigen concentration increases, the immune complex formed on the sensing interface can effectively prevent the diffusion pathway of the substrate to the signal interface, resulting in reducing the response current and the amount of blue product in the colorimetric reaction. Fig. 5A shows the relationship between the DPV response and the HBs Ag concentration with a low detection limit of 10.2 fg/mL in the linear range from 32 fg/mL to 100 ng/mL. Fig. 5C shows the relationship between the UV–vis absorbance and the HBs Ag concentration with a low detection limit of 3.3 pg/mL in the linear range from 10 pg/mL to 100 ng/mL. The linear equation of electrochemical method is: $I = -11.34\ lgC + 44.43$ with a correlation coefficient of 0.9975 (Fig. 5B). I (μA) and C (ng/mL) represent current and HBs Ag concentration, respectively. The linear equation of colorimetric method is: $Ab = -0.29\ lgC + 0.62$ with a correlation coefficient of 0.9868 (Fig. 5D). Ab and C (ng/mL) represent UV–vis absorbance at 652 nm and HBs Ag concentration, respectively. Electrochemical methods show lower detection limits than colorimetric sensing, directly suggesting the advantages of electrochemical sensors. To evaluate sensor performance, we compared different assays in previously reported HBs Ag assays and found that our electrochemical immunosensors showed lower detection limits (Table S3).

3.6. Reproducibility, specificity and stability

Reproducibility, selectivity and stability are important for the evaluation of immunosensors. Therefore, the reproducibility of immunosensors was studied for five different electrodes prepared by 31.7 fg/mL HBs Ag. The relative standard deviation (RSD) of the five electrodes was found to be 0.63%, indicating good reproducibility and high precision of the immunosensor (Fig. 6A). When 50 ng/mL different interfering substances: immunoglobulin G (IgG), BSA, carcinoembryonic antigen (CEA) and alpha-fetoprotein (AFP) were added to a solution of 31.7 fg/mL HBs Ag to study the specificity of immunosensors, the RSD of current signal was 1.1%, indicating the prepared electrochemical immunosensor has good specificity. Moreover, the interfering substances were added separately as a control experiment, with small signal, further eliminating the influence of interfering substances (Fig. 6B). The stability of prepared immunosensors can be assessed by checking the magnitude of its current signal every other week. As shown in Fig. 6C, the current response decreased slightly from 100% to 95.4% after four weeks, indicating good stability. The above results indicate that the proposed immunosensor has good reproducibility, specificity and stability for quantitative detection of HBs Ag. Detailed information on the experimental conditions is provided in the supplemental material.

3.7. Determination of HBs Ag in human serum

In order to study the feasibility of electrochemical immunosensors for detecting actual samples, the concentration of HBs Ag in the three serum samples was determined by standard addition method (Ruecha et al., 2019). We added 1.00 ng/mL, 5.00 ng/mL and 10.00 ng/mL HBs Ag solution to human serum samples. The relative standard deviation was from 2.40% to 3.44%, and the recovery rate was from 98.40% to 100.76%, showing the accuracy of the immunosensor. To further verify

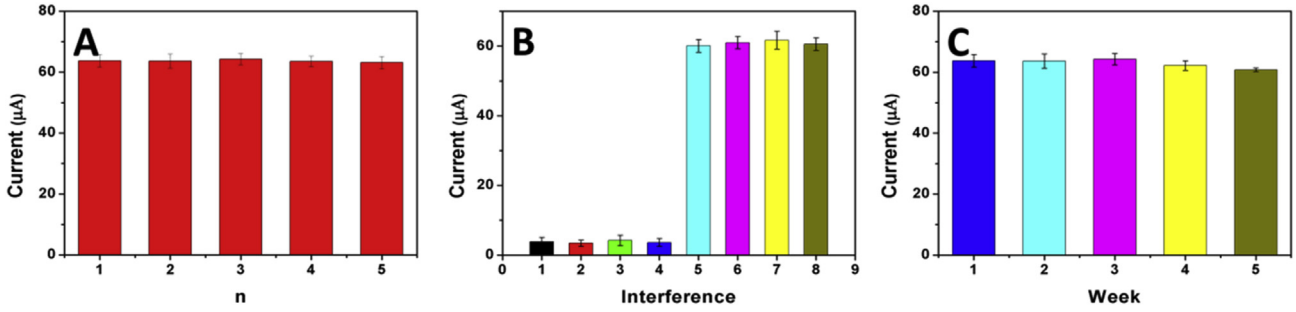

Fig. 6. (A) DPV current response of immunosensors for different electrodes treated in the same way (1–5) for reproducibility study; (B) Current response of individual interfering substances (50 ng/mL) (1) IgG, (2) BSA, (3) CEA and (4) AFP, (5, 6, 7, 8) interfering substances (50 ng/mL) and HBs Ag mixture (31.7 fg/mL); (C) The stability of the immunosensor tested at 31.7 fg/mL HBs Ag.

the accuracy of the proposed immunosensor, a comparison of electrochemical immunosensors with commercial ELISA methods (Lequin, 2005) is provided in Table S4. The results show that the relative deviation between the two methods ranges from −1.75% to 2.22%, indicating that there was no significant difference between the two methods for the detection of these three samples. Therefore, the label-free immunosensor we prepared may be a more accurate detection method for the determination of HBs Ag in clinical serum.

4. Conclusions

We have creatively synthesized PtPd NCs@MoS_2 nanoenzymes with enhanced catalytic activity as a signal amplification platform to realize quantitative detection of HBs Ag. PtPd NCs@MoS_2 nanoenzymes can effectively capture biomolecules and amplify current signals. The label-free immunosensor based on PtPd NCs@MoS_2 shows good specificity, reproducibility and stability. By analysis and comparison, the electrochemical method shows a lower detection limit (10.2 fg/mL) and a wider linear range (32 fg/mL to 100 ng/mL) than the colorimetric method (3.3 pg/mL and 10 pg/mL to 100 ng/mL). Therefore, the proposed electrochemical immunosensor is of great significance for accurate and rapid detection of HBs Ag, early detection of liver cancer and reduction of treatment costs.

CRediT authorship contribution statement

Zhaoling Tan: Conceptualization, Methodology, Software, Data curation, Writing - original draft. **Hui Dong:** Software, Validation. **Qing Liu:** Supervision. **Hui Liu:** Writing - review & editing. **Pingping Zhao:** Writing - review & editing. **Ping Wang:** Supervision. **Yueyun Li:** Supervision. **Daopeng Zhang:** Writing - review & editing. **Zengdian Zhao:** Visualization, Investigation, Validation. **Yunhui Dong:** Writing - review & editing.

Acknowledgment

We greatly appreciate the support of the National Natural Science Foundation of China (21405095; 21575079; 21671121) and the Shandong Provincial Natural Science Foundation (ZR2018MB008, ZR2018MB012).

Appendix A. Supplementary data

Supplementary data to this article can be found online at https://doi.org/10.1016/j.bios.2019.111556.

References

Alzahrani, F.M., Shaikh, S.S., Alomar, A.I., Acharya, S., Elhadi, N., 2019. Prevalence of hepatitis B virus (HBV) among blood donors in eastern Saudi arabia: results from a five-year retrospective study of HBV seromarkers. Ann. Lab. Med. 39 (1), 81–85.
Carla, O., 2002. Sensitive detection of HBsAg mutants by a gap ligase chain reaction assay. J. Clin. Microbiol. 40 (7), 2566.
Cho, K.H., Shin, D.H., Oh, J., An, J.H., Lee, J.S., Jang, J., 2018. Multidimensional conductive nanofilm-based flexible aptasensor for ultrasensitive and selective HBsAg detection. ACS Appl. Mater. Interfaces 10 (34), 28412–28419.
Duan, K., Du, Y., Feng, Q., Ye, X., Hong, X., Xue, M., Wang, C., 2014. Synthesis of platinum nanoparticles by using molybdenum disulfide as a template and its application to enzyme-like catalysis. ChemCatChem 6 (7), 1873–1876.
Francesco, B., Luigi, C., Guihua, Y., Meryl, S., Valentina, T., Ferrari, A.C., Ruoff, R.S., Vittorio, P., 2015. 2D materials. Graphene, related two-dimensional crystals, and hybrid systems for energy conversion and storage. Science 347 (6217), 1246501.
Gao, J., Du, B., Zhang, X., Guo, A., Zhang, Y., Wu, D., Ma, H., Wei, Q., 2014. Ultrasensitive enzyme-free immunoassay for squamous cell carcinoma antigen using carbon supported Pd–Au as electrocatalytic labels. Anal. Chim. Acta 833, 9–14.
Gomathi, T., Rajeshwari, K., Kanchana, V., Sudha, P., Parthasarathy, K., 2019. Impact of nanoparticle shape, size, and properties of the sustainable nanocomposites. In: Sustainable Polymer Composites and Nanocomposites. Springer, pp. 313–336.
Gourmelon, E., Lignier, O., Hadouda, H., Couturier, G., Bernède, J.C., Tedd, J., Pouzet, J., Salardenne, J., 2017. MS_2 (M = W, Mo) photosensitive thin films for solar cells. Sol. Energy Mater. Sol. Cells 46 (2), 115–121.
He, W., Jia, H., Li, X., Lei, Y., Li, J., Zhao, H., Mi, L., Zhang, L., Zheng, Z., 2012. Understanding the formation of CuS concave superstructures with peroxidase-like activity. Nanoscale 4 (11), 3501–3506.
Hu, H.-H., Liu, J., Chang, C.-L., Jen, C.-L., Lee, M.-H., Lu, S.-N., Wang, L.-Y., Quan, Y., Xia, N.-S., Chen, C.-J., 2019. Level of hepatitis B (HB) core antibody associates with seroclearance of HBV DNA and HB surface antigen in HB e antigen-seronegative patients. Clin. Gastroenterol. Hepatol. 17 (1), 172–181 e171.
Jia, H., Yang, D., Han, X., Cai, J., Liu, H., He, W., 2016. Peroxidase-like activity of the Co_3O_4 nanoparticles used for biodetection and evaluation of antioxidant behavior. Nanoscale 8 (11), 5938–5945.
Jiang, K., Nie, D., Huang, Q., Fan, K., Tang, Z., Wu, Y., Han, Z., 2019. Thin-layer MoS_2 and thionin composite-based electrochemical sensing platform for rapid and sensitive detection of zearalenone in human biofluids. Biosens. Bioelectron. 130, 322–329.
Kai, C., Zhicheng, L., Kun, C., Liang, H., Jing, W., Feng, S., Yanjun, W., Heyou, H., 2013. Aqueous synthesis of porous platinum nanotubes at room temperature and their intrinsic peroxidase-like activity. Chem. Commun. 49 (54), 6024–6026.
Lequin, R.M., 2005. Enzyme immunoassay (EIA)/enzyme-linked immunosorbent assay (ELISA). Clin. Chem. 51 (12), 2415–2418.
Li, F., Feng, J., Gao, Z., Shi, L., Wu, D., Du, B., Wei, Q., 2019. Facile synthesis of Cu_2O@TiO_2-PtCu nanocomposites as a signal amplification strategy for the insulin detection. ACS Appl. Mater. Interfaces 11 (9), 8945–8953.
Li, R., Zhen, M., Guan, M., Chen, D., Zhang, G., Ge, J., Gong, P., Wang, C., Shu, C., 2013. A novel glucose colorimetric sensor based on intrinsic peroxidase-like activity of C60-carboxyfullerenes. Biosens. Bioelectron. 47, 502–507.
Liu, F., He, J., Zeng, M., Hao, J., Guo, Q., Song, Y., Wang, L., 2016. Cu–hemin metal-organic frameworks with peroxidase-like activity as peroxidase mimics for colorimetric sensing of glucose. J. Nanoparticle Res. 18 (5), 1–9.
Ma, C., Ma, Y., Sun, Y., Lu, Y., Tian, E., Lan, J., Li, J., Ye, W., Zhang, H., 2019. Colorimetric determination of Hg^{2+} in environmental water based on the Hg^{2+}-stimulated peroxidase mimetic activity of MoS_2-Au composites. J. Colloid Interface Sci. 537, 554–561.
Makuza, J.D., Rwema, J.O.T., Ntihabose, C.K., Dushimiyimana, D., Umutesi, J., Nisingizwe, M.P., Serumondo, J., Semakula, M., Riedel, D.J., Nsanzimana, S., 2019. Prevalence of hepatitis B surface antigen (HBsAg) positivity and its associated factors in Rwanda. BMC Infect. Dis. 19 (1), 381.
Ott, J.J., Stevens, G.A., Groeger, J., Wiersma, S.T., 2012. Global epidemiology of hepatitis B virus infection: new estimates of age-specific HBsAg seroprevalence and endemicity. Vaccine 30 (12), 2212–2219.
Pei, F., Wang, P., Ma, E., Yang, Q., Yu, H., Gao, C., Li, Y., Liu, Q., Dong, Y., 2019. A sandwich-type electrochemical immunosensor based on RhPt NDs/NH2-GS and Au NPs/PPy NS for quantitative detection hepatitis B surface antigen. Bioelectrochemistry 126, 92–98.
Ruecha, N., Shin, K., Chailapakul, O., Rodthongkum, N., 2019. Label-free paper-based electrochemical impedance immunosensor for human interferon gamma detection.

Sens. Actuators B Chem. 279, 298–304.
Shi, Y.-C., Feng, J.-J., Lin, X.-X., Zhang, L., Yuan, J., Zhang, Q.-L., Wang, A.-J., 2019. One-step hydrothermal synthesis of three-dimensional nitrogen-doped reduced graphene oxide hydrogels anchored PtPd alloyed nanoparticles for ethylene glycol oxidation and hydrogen evolution reactions. Electrochim. Acta 293, 504–513.
Singh, A.K., Kumar, P., Late, D., Kumar, A., Patel, S., Singh, J., 2018. 2D layered transition metal dichalcogenides (MoS2): synthesis, applications and theoretical aspects. Appl. Mater. Today 13, 242–270.
Wang, C., Daimon, H., Onodera, T., Koda, T., Sun, S., 2008. A general approach to the size-and shape-controlled synthesis of platinum nanoparticles and their catalytic reduction of oxygen. Angew. Chem. Int. Ed. 47 (19), 3588–3591.
Wang, X.X., Wu, Q., Shan, Z., Huang, Q.M., 2011. BSA-stabilized Au clusters as peroxidase mimetics for use in xanthine detection. Biosens. Bioelectron. 26 (8), 3614–3619.
Wang, Y., Wang, Y., Dan, W., Ma, H., Yong, Z., Fan, D., Pang, X., Du, B., Qin, W., 2018. Label-free electrochemical immunosensor based on flower-like Ag/MoS_2/rGO nanocomposites for ultrasensitive detection of carcinoembryonic antigen. Sens. Actuators B Chem. 255.
Wang, Z., Lin, J., Gao, J., Wang, Q., 2016. Two optically active molybdenum disulfide quantum dots as tetracycline sensors. Mater. Chem. Phys. 178, 82–87.
Yamada, M., 2009. Synthesis of organic shell–inorganic core hybrid nanoparticles by wet process and investigation of their advanced functions. Bull. Chem. Soc. Jpn. 82 (2), 152–170.
Yan, Q., Cao, L., Dong, H., Tan, Z., Hu, Y., Liu, Q., Liu, H., Zhao, P., Chen, L., Liu, Y., 2019a. Label-free immunosensors based on a novel multi-amplification signal strategy of TiO_2-NGO/Au@Pd hetero-nanostructures. Biosens. Bioelectron. 127, 174–180.
Yan, Q., Cao, L., Dong, H., Tan, Z., Liu, Q., Zhang, W., Zhao, P., Li, Y., Liu, Y., Dong, Y., 2019b. Sensitive amperometric immunosensor with improved electrocatalytic Au@Pd urchin-shaped nanostructures for human epididymis specific protein 4 antigen detection. Anal. Chim. Acta 1069, 117–125.
Yan, Q., Yang, Y., Tan, Z., Liu, Q., Liu, H., Wang, P., Chen, L., Zhang, D., Li, Y., Dong, Y., 2018. A label-free electrochemical immunosensor based on the novel signal amplification system of AuPdCu ternary nanoparticles functionalized polymer nanospheres. Biosens. Bioelectron. 103, 151–157.
Yang, Y., Liu, Q., Liu, Y., Cui, J., Liu, H., Wang, P., Li, Y., Chen, L., Zhao, Z., Dong, Y., 2017. A novel label-free electrochemical immunosensor based on functionalized nitrogen-doped graphene quantum dots for carcinoembryonic antigen detection. Biosens. Bioelectron. 90, 31–38.
Yang, Y., Yan, Q., Liu, Q., Li, Y., Liu, H., Wang, P., Chen, L., Zhang, D., Li, Y., Dong, Y., 2018. An ultrasensitive sandwich-type electrochemical immunosensor based on the signal amplification strategy of echinoidea-shaped Au@Ag-Cu_2O nanoparticles for prostate specific antigen detection. Biosens. Bioelectron. 99, 450–457.
Yu, F., Yao, D., Qian, W., 2000. Reflectometry interference spectroscopy in detection of hepatitis B surface antigen. Clin. Chem. 46 (9), 1489.
Zhang, L., Xie, X., Yuan, Y., Chai, Y., Yuan, R., 2019. FeS_2-AuNPs nanocomposite as mimicking enzyme for constructing signal-off sandwich-type electrochemical immunosensor based on electroactive nickel hexacyanoferrate as matrix. Electroanalysis 31 (6), 1019–1025.